TRANSITION METAL SULFIDES FOR ELECTROCHEMICAL APPLICATIONS: CONTROLLED CHEMICAL CONVERSION OF CuS TO Ag_2S

Julia M. Mazurków[a,], Anna Kusior[a], Andrzej Mikuła[a], Marta Radecka[a]*

[a] Faculty of Materials Science and Ceramics, AGH University of Science and Technology, al. Adama Mickiewicza 30, 30-059 Krakow, Poland

Corresponding Author

* e-mail: mazurkow@agh.edu.pl, Phone: +48 12 617 24 68

ABSTRACT

Transition metal sulfides have received great attention as electrocatalysts for electrochemical sensors and water electrolysis. In the present study, a facile and rapid chemical conversion route was used for the synthesis of partially and fully converted Ag_2S from tube-like CuS. The morphology of the obtained materials was investigated by scanning electron microscopy (SEM) and transition electron microscopy (TEM), revealing that the complex shape of CuS was maintained after the conversion. Information about phase and elemental composition was obtained by X-ray diffraction (XRD), Raman spectroscopy, X-ray fluorescence spectrometry (XRF), and inductively coupled plasma optical emission spectrometry (ICP-OES). The surface composition was analyzed utilizing X-ray photoelectron spectroscopy (XPS). The results indicated that it was possible to precisely control the contribution of each sulfide by varying precursors ratio. Moreover, the conducted experiments enabled to schematically illustrate the CuS-Ag_2S junction and propose a conversion mechanism. The electrochemical behavior of the materials was examined using cyclic voltammetry (CV) in the potential range of biomolecules electrooxidation as well as water splitting. Special attention was devoted to reactions occurring on Ag_2S-modified electrodes in alkaline and neutral media. It was found that the formation of subsequent oxides, their reduction, and the recovery of Ag_2S are diffusion-controlled processes.

KEYWORDS: silver sulfide, copper sulfide, chemical conversion, cation exchange, electrochemical behavior

1. Introduction

Electrochemistry remains a very active area of both fundamental and application research. A vast number of currently developed sustainable technologies are based on redox reactions. This includes fuel cells, supercapacitors, batteries, electrochemical sensors, and photoelectrochemical cells. Among materials exhibiting interesting electrochemical properties, transition metal sulfides (TMS) have attracted significant attention [1,2]. The electrocatalytic activity of TMS is considered to be greater than that of appropriate oxides and hydroxides due to their higher electronic conductivity [3–5]. Moreover, this group of materials possess rich redox chemistry and unique electronic structures [6]. To fully exploit the material potential as an electrocatalyst, the evaluation of the basic processes occurring at the electrode-electrolyte interface remains crucial. The electrochemical behavior of metals in alkaline solutions has been extensively studied in terms of their application in electrochemical sensors [7–9], as well as water splitting [10,11]. However, for metal sulfides, a basic understanding of the interactions between the material and the electrolyte is still lacking.

Acanthite (monoclinic Ag_2S) is a narrow band gap semiconductor (~0.9 eV). It has been investigated as an electrode material for a wide range of electrochemical applications, such as electrochemical biosensors [12,13], gas sensors [14,15], and water electrolysis [16,17]. Moreover, silver sulfide has also been used to enhance the electrocatalytic performance of other sulfides such as CuS, CoS, or MoS_2 [5,18–20].

In our previous work [21,22], we have shown, based on the example of electrodes for photoelectrochemistry, that the activity of heterostructures is determined by the morphology and physicochemical properties of the constituents. Therefore, it is important to consider their architecture in the material design process. Among the proposed techniques for the synthesis of Ag_2S, chemical conversion offers certain unique features. This method extends the available

morphologies for silver sulfide and enables to benefit from the abundance of possible shapes of other compounds such as copper sulfides. For example, Basu et al. utilized CuS with two different morphologies, flower balls and wires, as sacrificial templates for the synthesis of Ag_2S/Ag heterostructures [23]. Furthermore, chemical conversion can aid in shaping the interface between converted materials. In the study by Tan et al., sequential cation exchange of CdS to Cu_2S and further to Ag_2S induced the preferential nucleation of silver sulfide along the twin boundaries that were created in the first stage of the process [24]. By varying the reaction time, it was possible to roughly tune the length of the Ag_2S segments. This indicates that the degree of conversion can be adjusted. However, the strictly quantitative approach as well as a more feasible way of precise control over the phase composition have not been investigated yet. Another challenging issue remains the conversion of hierarchical microstructures while retaining their morphology.

In this work, we propose a facile and rapid chemical conversion route of CuS to Ag_2S at room temperature. By simply varying CuS:$AgNO_3$ ratio, it was possible to gain control over the final composition of the powders and at the same time retain the complex morphology of the starting material. Partial as well as full conversion were achieved. Detailed studies were devoted to describing the junction between copper and silver sulfide. In addition, the origins of trace amounts of silver in converted Ag_2S were discussed. The electrochemical behavior of the obtained materials was investigated to provide a firm theoretical background for their application as electrocatalysts in an alkaline and neutral medium.

2. Materials and methods

2.1 Materials

Ethylene glycol (EG, $C_2H_6O_2$), silver nitrate ($AgNO_3$), and sodium hydroxide solution (0.1 M NaOH) were purchased from Avantor. Copper sulfate ($CuSO_4 \cdot 5H_2O$) was provided by Chempur and sodium thiosulfate pentahydrate ($Na_2S_2O_3 \cdot 5H_2O$) by Acros Organics. Polyvinylpyrrolidone (PVP, M.W. 40 000) was supplied by Alfa Aesar. Phosphate buffered saline (PBS) tablets, Sigma, were used. All solutions were prepared using deionized water.

2.2 Synthesis of CuS

For the synthesis of copper sulfide, the method proposed by Kundu et al. [25] was used with certain alterations. As a copper precursor served $CuSO_4 \cdot 5H_2O$ (0.05 mM) and as a sulfur precursor – $Na_2S_2O_3 \cdot 5H_2O$ (0.05 mM). They were mixed for 2 h in a solution of water (50 mL) and ethylene glycol (150 mL) cooled to 1 °C in an ice bath. Subsequently, the reaction mixture was left at room temperature for 4 weeks. After this time, the black precipitate was separated from the solution by centrifugation and washed with a water/ethanol mixture (50 vol.%/50 vol.%) three times. The powder was dried in a vacuum dryer at 60 °C for 12 h.

2.3 Chemical conversion of CuS to Ag_2S

Copper sulfide was converted to silver sulfide by a cation exchange process. As obtained CuS powder was suspended in 25 mL of ethylene glycol using ultrasounds for 1 min. Then a solution of silver nitrate in ethylene glycol (25 mL) was added to the CuS suspension and everything was mixed for 1 min on the magnetic stirrer. The variable was the molar ratio of CuS to $AgNO_3$ (see Table 1). The powder was separated from the solution by 5 min of centrifugation and subsequently washed with a water/ethanol mixture (50 vol.%/50 vol.%) three times. The product was dried in the vacuum dryer at 25 °C for 12 h. Additionally, three conversion processes were

conducted with a set nCu:nAg molar ratio of 1:2, but with variable other parameters - overall concentration, solvent, and type of laboratory glass (Table 1). For comparison purposes, pure Ag_2S was obtained following the same procedure as for copper sulfide, but with silver nitrate as a silver precursor.

Table 1. Composition of suspensions used for chemical conversion.

Sample	nCuS / mmol	$nAgNO_3$ / mmol	nCu:nAg	Remarks
CA_4:1	4.00	1.00	4:1	standard procedure
CA_2:1	3.35	1.65	2:1	standard procedure
CA_1:2	1.65	3.35	1:2	standard procedure
AC_1:2	0.63	1.25	1:2	decreased concentrations
WW_1:2	1.65	3.35	1:2	water used as a solvent
AG_1:2	1.65	3.35	1:2	amber volumetric flask

2.4 Characterization of materials

The surface morphology of the obtained materials was analyzed by scanning electron microscopy (SEM, Nova NanoSEM 200, FEI Company). A specific surface area assessment utilizing the Brunaer-Emmet-Teller (BET) method was carried out on the ASAP 2020 Plus Adsorption Analyzer, Micrometrics. The degassing temperature was 150 °C. The phase composition was determined by X-ray diffraction (XRD). Spectra were collected using the X'Pert MPD diffractometer, Malvern Panalytical Ltd., with the Johansson monochromator (Cu $K\alpha_1$ radiation, 1.5406 Å). Rietveld refinement was performed using HighScore Plus software, Malvern Panalytical Ltd. Raman spectroscopy measurements were conducted on the Raman confocal microscope alpha 300R, WITec GmbH. The excitation wavelength was 488 nm and the objective 50x was used. The integration time was set to 20 s and the accumulation number to 5. The presented spectra are the average of three independent measurements. For wavelength

dispersive X-ray fluorescence spectrometry (WDXRF), the Axios mAX spectrometer, Malvern Panalytical Ltd., with the Rh lamp (4 kW) was employed. For inductively coupled plasma optical emission spectrometry (ICP-OES) experiments served Optima 7300DV ICP-OES spectrometer, Perkin Elmer. The powder samples were mineralized in concentrated HNO_3 at 230 °C and 68 bar. Surface composition was evaluated by X-ray photoelectron spectroscopy (XPS), PHI5000 VersaProbe II Scanning XPS Microprobe, Physical Electronics. Monochromatic Al Kα (1486.6 eV) was utilized as an X-ray source. The area of analysis was 400 µm x 400 µm and the depth of analysis around 5 nm. Detailed information on the materials structure provided transmission electron microscopy (TEM) performed on Tecnai TF 20 X-TWIN, FEI Company.

2.5 Preparation of the electrodes

Glassy carbon electrodes (GCE) were modified with the obtained materials using a drop casting method as described previously [26]. Briefly, 12.5 mg of appropriate powder were added to 5 ml of aqueous solution containing 50 mg of PVP. Subsequently, the suspension was homogenized by mixing on the magnetic stirrer for 30 min and applying ultrasounds for 10 min. A drop of 10 µl was then casted onto the activated GCE surface and left for drying. When not in use, electrodes were stored in the refrigerator suspended over the deionized water.

2.6 Electrochemical measurements

To investigate the electrochemical properties of the modified electrodes, cyclic voltammetry (CV) was used. CV measurements were performed in a three electrode system on the electrochemical analyzer M161E, MTM Anko. The role of a working electrode played modified GCE, as a reference electrode served Ag/AgCl (3 M KCl) and as an auxiliary – platinum wire (Pt). All electrodes were provided by Mineral. The experiments were conducted in 15 mL of appropriate electrolyte - 0.1 M NaOH or 0.1 M PBS.

3. Results and Discussion

3.1 Morphology and structure characterization

The morphology of synthesized CuS, converted materials (CA_4:1, CA_2:1 and CA_1:2) and Ag_2S can be seen in Fig. 1. Tube-like copper sulfides with diameter and height of around 1 μm were filled with clusters of spherical particles loosely tied with the hexagonal shell. After subsequent conversion, the powders retained their morphology, indicating the perfect structural stability of the tubes. In the case of the directly obtained silver sulfide, it was composed of agglomerated nanosized particles. The powders changed their color from bottle green to gray for pure CuS and Ag_2S, respectively (Fig. S1). The specific surface area determined using the BET method for the initial CuS powder was 7.4 m^2/g (the obtained isotherm is presented in Fig. S2).

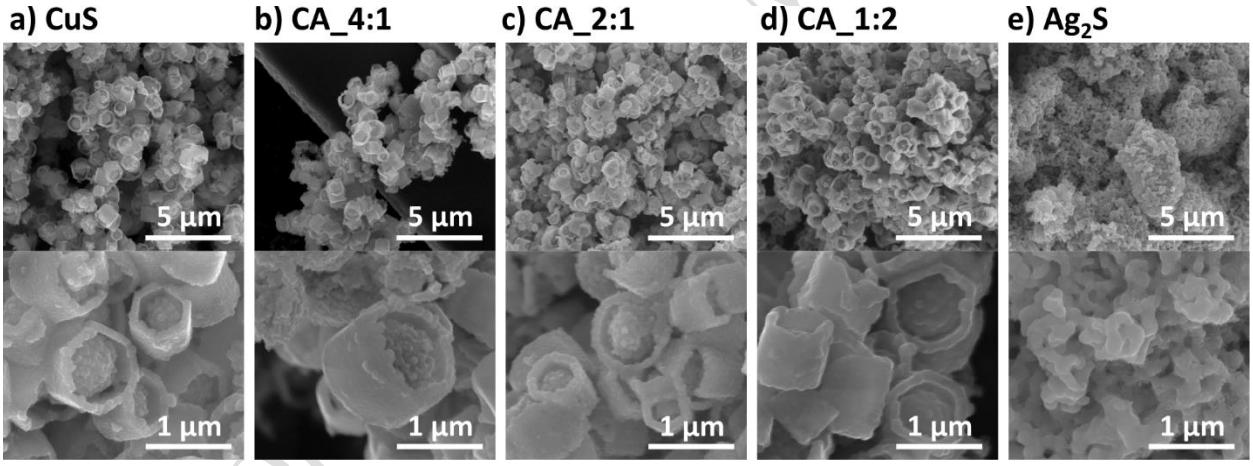

Figure 1. SEM images of CuS (a), CA_4:1 (b), CA_2:1 (c), CA_1:2 (d) and Ag_2S (e).

XRD analysis (Fig. 2a) revealed the presence of a pure covellite phase (hexagonal, space group: $P6_3/mmc$, JCPDS no. 98-006-1792) within the CuS sample. Upon its successive conversion to silver sulfide and decreased molar ratio of Cu:Ag, the presence of an acanthite phase (monoclinic, space group: $P2_1/c$, JCPDS no. 98-004-4507) become more pronounced. These results were supported by Raman spectroscopy (Fig. 2b). In the spectrum for CuS, two bands were observed at 265 and 472 cm^{-1}, which can be assigned to Cu-S and S-S bonds,

respectively, within copper sulfide. These bands were diminished for converted samples and disappeared in the case of CA_1:2 and Ag_2S. On the other hand, the emerging broad bands in the range of 100-300 cm^{-1} indicated an increasing content of silver sulfide [27].

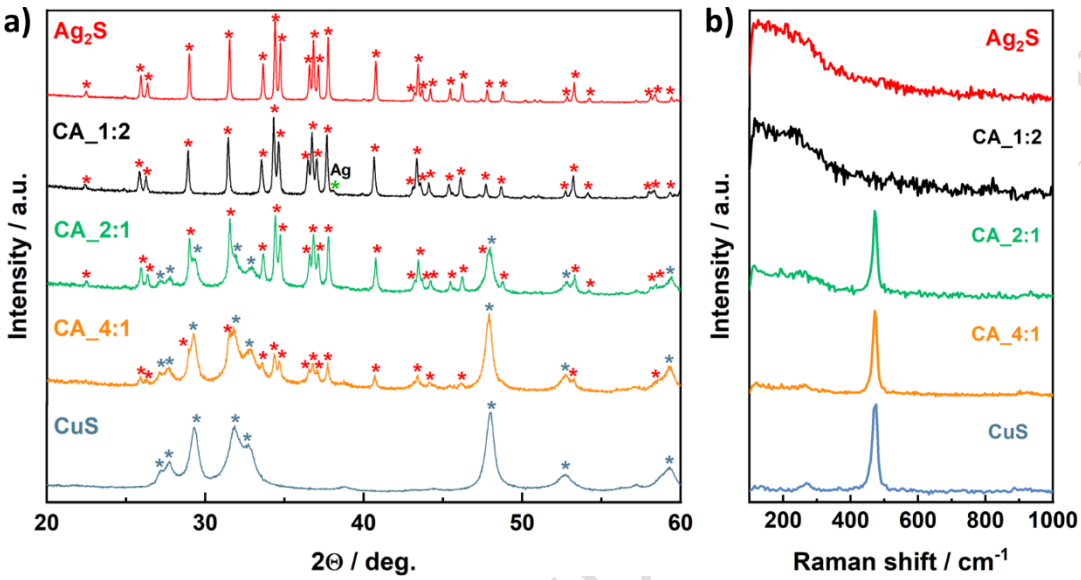

Figure 2. XRD patterns for all samples (a). Peaks characteristic for covellite are marked with blue stars and for acanthite with red ones. Raman spectra versus normalized intensity for all samples (b).

To determine the phase composition of each of the converted samples, Rietveld refinement was performed. It revealed that in the case of CA_4:1, CuS:Ag_2S ratio was 78:22 wt.% (theoretical 73:27 wt.%) and for CA_2:1 the ratio was 56:44 wt.% (theoretical 54:46 wt.%). For CA_1:2, no covellite phase was detected. However, small amount (2 wt.%) of metallic silver (cubic, JCPDS no. 01-087-0717) was present. Importantly, no shifts in the diffractograms characteristic for doped materials were observed. These results indicate that the proposed conversion process is highly controllable. The calculated crystallite size for CuS based on the Scherrer equation increased from 12±3 nm to 24±4 nm (CuS and CA_2:1 samples, respectively). On the other hand, the crystallite size of Ag_2S was the largest in pure silver sulfide (141±4 nm)

and decreased when the degree of conversion was lower (54±2 nm for CA_4:1). The evaluated phase compositions and crystallite size values are summarized in Table 2.

Table 2. Summary of the phase composition, crystallite sizes determined for CuS and Ag_2S, and Cu:Ag molar ratio in the samples given as a weight percentage.

Sample	CuS:Ag_2S / wt.%		Crystallite size / nm		Cu:Ag / wt.%		
	theoretical	XRD	CuS	Ag_2S	theoretical	WDXRF	ICP-OES
CuS	100:0	100:0	12±3	-	-	-	-
CA_4:1	73:27	78:22	16±3	54±2	67:33	69:31	67:33
CA_2:1	54:46	56:44	24±4	75±6	47:53	47:53	46:54
CA_1:2	0:100	0:100*	-	83±4	0:100	2:98	1:99
Ag_2S	0:100	0:100	-	141±4	-	-	-

* without considering the presence of metallic silver

Based on XRD and Raman spectroscopy, it was concluded that the CA_4:1 and CA_2:1 samples are composed of CuS/Ag_2S, whereas CA_1:2 consists of Ag/Ag_2S and no residues of copper sulfide were detected. Additionally, no bands of copper sulfate were observed in the Raman spectra. To further investigate the composition of powders, WDXRF and ICP-OES measurements were carried out to determine Cu:Ag ratio in the converted powders. As can be seen in Table 2., the results of both measurements were convergent and supported conclusions drawn from XRD. The Cu:Ag ratio determined by WDXRF and ICP-OES for the CA_4:1 sample was 69:31 and 67:34 wt.% (theoretical 67:33 wt.%), respectively, and for CA_2:1 – 47:53 and 46:54 wt.% (theoretical 60:40 wt.%). In the case of CA_1:2, trace amounts of copper were detected (2 wt.% in WDXRF and 1 wt.% in ICP-OES).

3.2. XPS analysis

XPS analysis was used to study in detail the surface composition of the CA_2:1 and CA_1:2 samples. Special attention was devoted to the determination of the bonds between the elements.

In the Ag 3d high-resolution spectra (Fig. 3a,d), two well-defined symmetrical lines centered at 374.8 and 368.8 eV ($d_{3/2}$-$d_{5/2}$ doublet, separated by 6.0 eV) were observed. These values were more positive compared to the line positions of Ag^+ in Ag_2S reported in the literature [28]. It can be explained by the presence of Ag^0 along with Ag^+ in both samples [16,29], as indicated by XRD. The line positions of metallic silver and silver ions in Ag_2S are too close to distinguish them properly in our spectra. The high-resolution Cu $2p_{3/2}$ spectrum for CA_2:1 presented in Fig. 3b was fitted with the two lines positioned at 932.7 eV (with an asymmetric tail) and 935.3 eV. They were attributed to Cu^+ as the major oxidation state of copper in covellite [30] and Cu-SO bonds in copper sulfate [28], respectively. In the spectrum for CA_1:2 (Fig. 3e) no lines specific for Cu-S bond in copper sulfide were detected. However, trace amounts of copper hydroxides and sulfates were identified. It was further proved by the three satellite lines within the energy range of 940 – 945 eV characteristic for Cu^{2+} shake-up processes in $Cu(OH)_2$ and $CuSO_4$ [28]. They might originate from the adsorbed byproducts of conversion. Analysis of the S 2p region for the CA_2:1 sample (Fig. 3c) revealed the presence of three $p_{3/2}$-$p_{1/2}$ doublets separated by 1.2 eV centered at 162.0 and 163.2 eV, 162.7 and 163.9 eV, 164.0 and 165.2 eV, which can be assigned to sulfides and polysulfides [31]. Such spectrum is typical for covellite due to the presence of S^{2-} and S_2^{2-} moieties within this compound [30,32]. Additionally, a doublet at 168.8 and 170.0 eV indicated the existence of sulfates on the powder surface [31]. As can be seen in Fig. 3f, only sulfides and sulfates lines were observed for the CA_1:2 sample, confirming the complete conversion. The survey spectra for both samples are presented in Fig. S3 and Fig. S4.

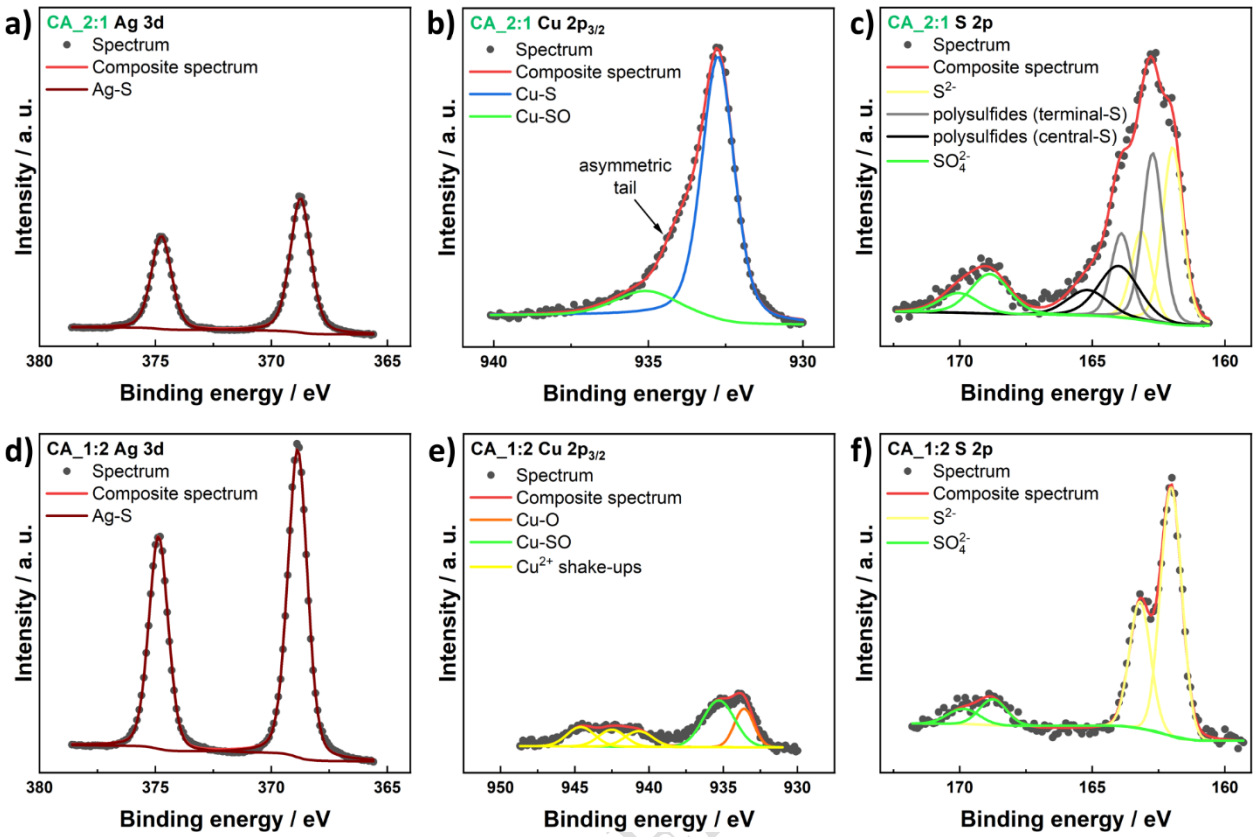

Figure 3. High-resolution XPS spectra of CA_2:1 (a,b,c) and CA_1:2 (d,e,f): Ag 3d (a,d), Cu $2p_{3/2}$ (b,e) and S 2p (c,f).

3.3. TEM analysis

TEM images further proved the specific morphology of the powders composed of a hexagonal tube-like shell and clusters of nanosized particles trapped inside (Fig. 4a). To investigate the distribution of the elements within the powder, energy-dispersive X-ray spectroscopy (EDS) was used. As can be seen in Fig. 4b, copper, sulfur and silver were present within the whole structures.

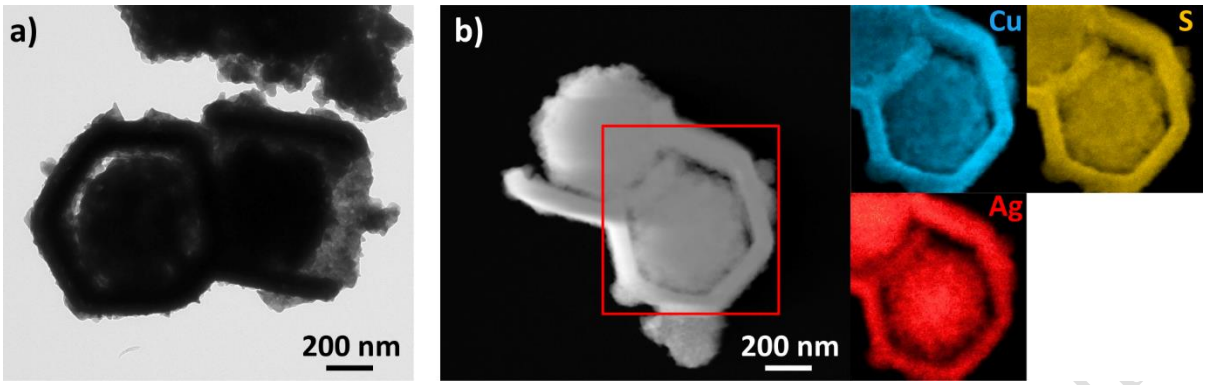

Figure 4. TEM image of the converted CA_2:1 sample (a) and dark-field image with EDS mapping of the region marked with the red frame (b).

The selected area electron diffraction (SAED) measurements of the region with a diameter of 3 µm were conducted (Fig. 5a). The obtained ring diffraction pattern is characteristic for polycrystalline samples (Fig. 5b). Based on the diameter of the fitted rings, the lattice spacings were determined and the corresponding CuS and Ag_2S planes were assigned to them (Table S1), confirming the presence of these two phases within the sample. Furthermore, high resolution TEM (HR-TEM) analysis was performed. It revealed that the (020) planes of monoclinic silver sulfide are parallel to the (002) planes of hexagonal copper sulfide (Fig. 5c). Based on this observation, we proposed a schematic illustration of the CuS-Ag_2S junction within converted samples (Fig. 5d).

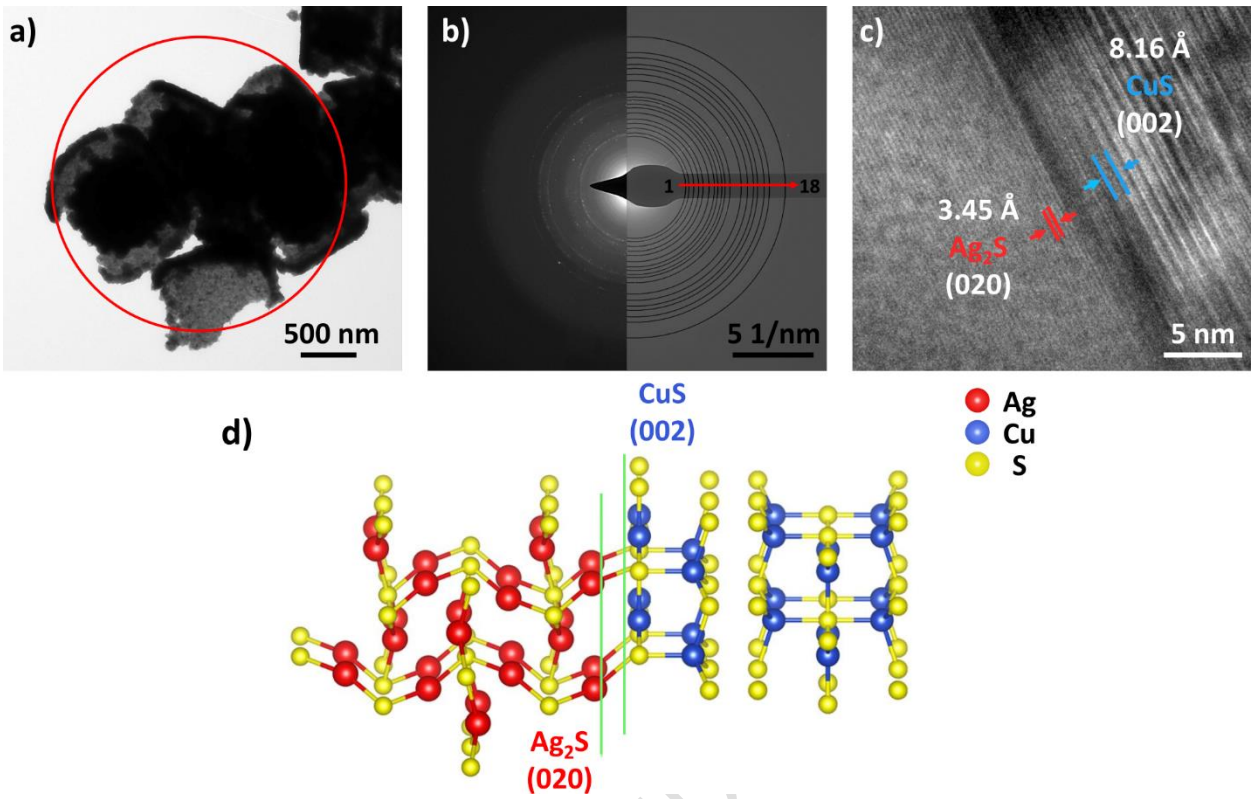

Figure 5. TEM image of the converted CA_2:1 sample (a), and the SAED pattern with numbered rings of the region marked with the red circle (b). HR-TEM image with marked d-spacing values of 3.45 Å and 8.16 Å assigned to the Ag_2S (020) plane and the CuS (002) plane, respectively (c). Schematic illustration of the CuS-Ag_2S junction with marked the (020) plane of Ag_2S and the (002) plane of CuS (d).

3.4. Conversion mechanism

The chemical conversion of CuS to Ag_2S is schematically presented in Fig. 6. Based on the results presented in sections 3.1 - 3.3 and TEM images under different magnifications (Fig. S5), it was proposed that the nucleation centers of Ag_2S were uniformly distributed throughout the whole structure and were spreading upon conversion. Although the theoretical volume expansion of the cell is 11% for this reaction, the complex tube-like shape was maintained. The cation-exchange reaction between Ag^+ and CuS is a thermodynamically favored process (the standard

enthalpy of formation for Ag^+ is 105.9 kJ/mol and for Cu^{2+} 64.4 kJ/mol). The reduction of silver ions to metallic silver observed in converted samples may have different origins: (1) excessive silver nitrate concentration in the conversion solution, (2) reducing effect of ethylene glycol [33], (3) UV light irradiation [34] or (4) redox reaction between Ag^+ and S^{2-} with Ag_2S acting as a catalyst [35]. To verify these hypotheses, additional conversion processes were performed for nCu:nAg = 1:2 (ratio of reactants). The products were analyzed using XRD and compared with the CA_1:2 sample. In the case of reduced $AgNO_3$ concentration from 67 to 25 mM (AC_1:2), using water as a solvent instead of EG (WW_1:2), as well as conducting experiment in an amber glass to eliminate UV irradiation (AG_1:2), the same amount of metallic silver (around 2 wt.%) was determined by Rietveld refinement in all samples. The appropriate XRD patterns are shown in Fig. S6. Therefore, it can be concluded that silver ions were slowly reduced by abundant S^{2-} as proposed by Motte et al. [35]. During conversion, lattice rearrangement occurred, and the sulfur coordination number changed from 4 in CuS to 5 in Ag_2S, which may explain the source of these excessive sulfide ions. Nonetheless, the reduction of Ag^+ was only a marginal process.

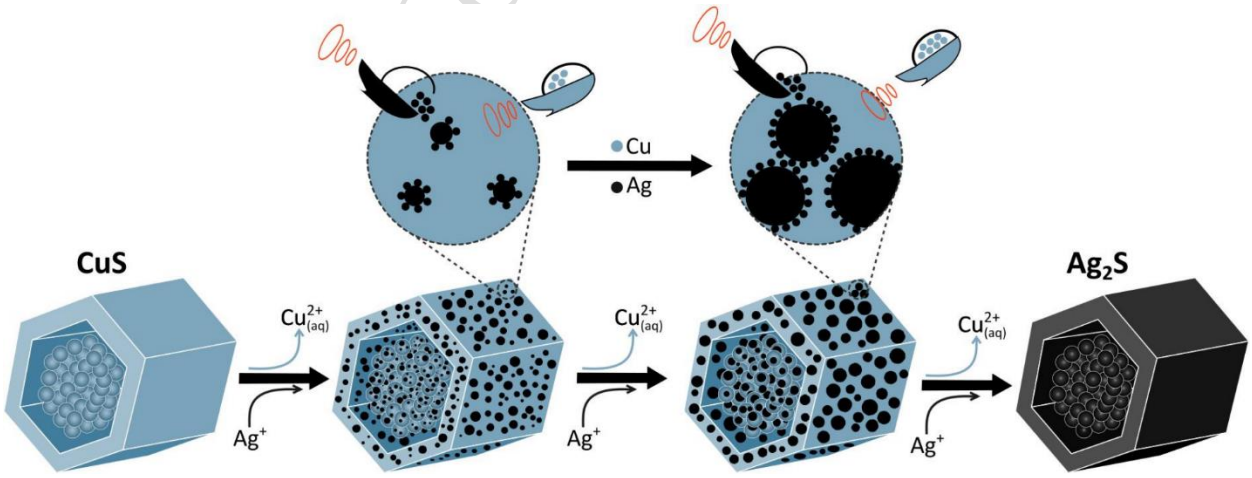

Figure 6. Proposed mechanism of CuS-Ag_2S chemical conversion involving expansion of the randomly distributed nucleation centers of silver sulfide.

3.5. Electrochemical behavior

The electrochemical behavior of compounds in alkaline electrolytes is of special importance in terms of their application in electrochemical sensors and for water splitting. Fig. 7 shows the cyclic voltammograms of the GCE modified with CuS, CA_4:1, and CA_2:1 measured in 0.1 M NaOH. For CuS/GCE, scanning with the increased speed (6.25 to 100 mV/s) did not significantly influence the curves and no peaks were recorded (Fig. 7a). This is in contrast to metallic copper-based electrodes for which peaks of subsequent oxidation $Cu^0 \rightarrow Cu^+ \rightarrow Cu^{2+} \rightarrow Cu^{3+}$ are clearly visible in an alkaline medium [8]. On the other hand, the presence of Ag_2S in the converted samples yielded five anodic peaks (one on the cathodic curve) and two cathodic peaks (Fig. 7b,c) characteristic only for silver [10]. Their signal increased with scan speed. What is interesting, in the case of Cu-Ag alloys studied by Assaf et al. [36], the cyclic voltammograms were composed of peaks originating from both copper and silver redox reactions.

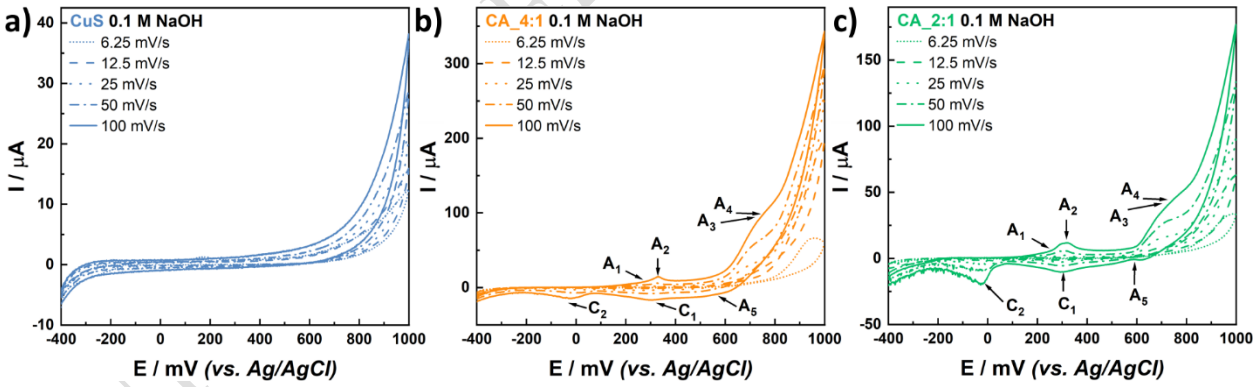

Figure 7. Cyclic voltammograms recorded at different scan rates (6.25 – 100 mV/s) for CuS/GCE (a), CA_4:1/GCE (b) and CA_2:1/GCE (c) in 0.1 M NaOH solution.

To better understand the origin of the emerging peaks, a detailed study was conducted on the behavior of CA_1:2/GCE (Fig. 8) and Ag_2S/GCE (Fig. S7) in different electrolytes. Both electrodes exhibited similar electrochemical behavior. The voltammograms recorded in 0.1 M

NaOH (Fig. 8a and Fig. S7a) consist of four anodic peaks (positive sweep), as well as two anodic and three cathodic peaks (negative sweep). When the electrodes were scanned in a positive direction, the two anodic peaks A_1 and A_2 appeared at 220 and 340 mV, respectively. Typically, for Ag-based electrodes, they are related to the electrodissolution of silver and the formation of silver oxide [10]. However, for Ag_2S materials, the formation of the hydroxide layer may be associated rather with a change in the adsorption mechanism. In the initial stage, when the electrode is immersed in the electrolyte, it is solvated by electrolyte molecules. As a result of surface/van der Waals forces, OH^- groups are adsorbed on the Ag_2S surface. After exceeding a certain potential, an Ag-O chemical bond is created, resulting in the release of sulfur ions and their subsequent hydrolysis (A_1 peak at 220 mV). The following A_2 peak at 340 mV can be ascribed to the formation of silver (I) oxide. The next stages involve electrooxidation to AgO (A_3 peak at 730 mV) and higher oxides such as Ag_2O_3 (A_4 peak at 790 mV). In the case of metallic silver as well as its alloys, Ag_2O_3 formation is not always observed [36–39]. The unusual anodic peaks emerging during the cathodic scan (A_5 at 680 mV and A_5' at 590 mV) also recorded for silver electrodes [10] are induced by a continuous growth of Ag_2O on native silver sulfide. The first cathodic peak C_1 at 360 mV is correlated with the reduction of AgO to Ag_2O, while peaks C_2 at -60 mV and C_2' at -120 mV arise from the Ag_2S regeneration. The above description is summarized as a list of peaks with proposed reactions in Table 3.

Table 3. The list of the detected peaks on the voltammograms for CA_1:2 sample, their potentials (vs. Ag/AgCl, 3M KCl), and corresponding reactions.

Peak	Potential / mV	Reaction
Anodic curve		
A_1	220	$Ag^+ + 2OH^- \leftrightarrow [Ag(OH)_2]^-_{ads}$ $[Ag(OH)_2]^-_{ads} \leftrightarrow [Ag(OH)_2]^-_{aq}$
A_2	340	$[Ag(OH)_2]^-_{aq} \leftrightarrow Ag_2O + H_2O$
A_3	730	$Ag_2O + 2OH^- \leftrightarrow 2AgO + H_2O + 2e^-$
A_4	790	$2AgO + 2OH^- \leftrightarrow Ag_2O_3 + H_2O + 2e^-$
Cathodic curve		
A_5	680	$2Ag^+ + 2OH^- \leftrightarrow Ag_2O + H_2O$
A'_5	590	
C_1	360	$2AgO + H_2O + 2e^- \leftrightarrow Ag_2O + 2OH^-$
C_2	60	$Ag_2O + +H_2O \leftrightarrow 2Ag^+ + 2OH^-$
C'_2	-120	

The current values of all major peaks increased linearly with the square root of the scan rate (Fig. 8c and Fig. S7c), proving diffusion-controlled processes. The mechanism of Ag_2O and AgO formation on silver electrodes was studied by Jovic et al. [11], who found that the kinetics of silver oxides formation and their morphological structure depend on the concentration of hydroxides. When NaOH concentrations lower than 1 M were applied, the growth process was controlled by diffusion and the phenomenon of nucleation.

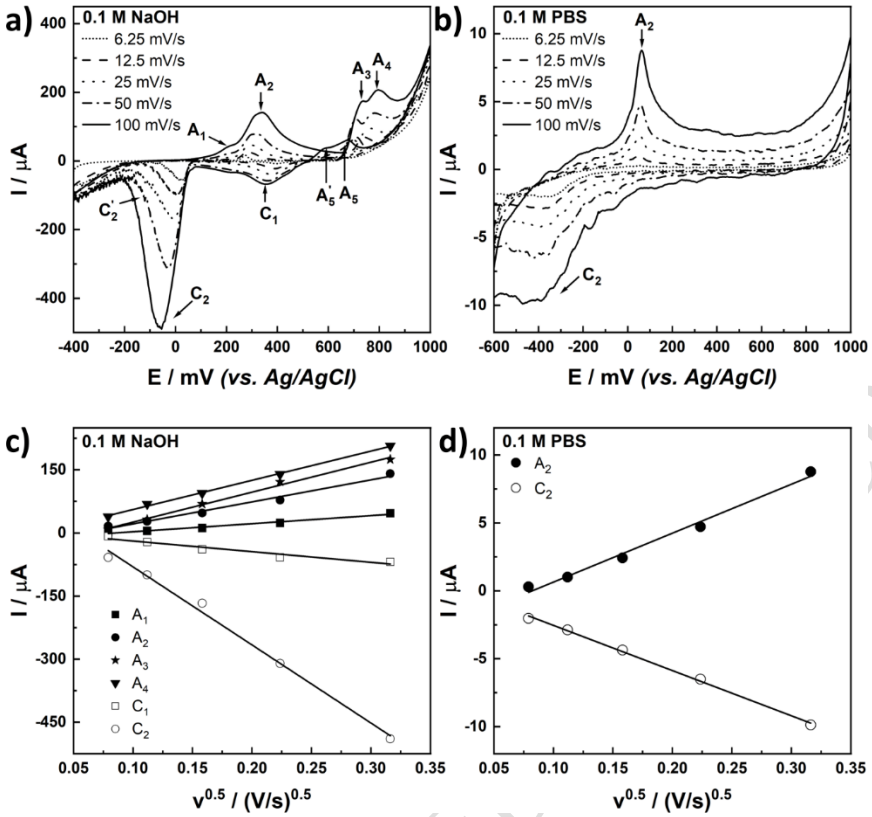

312

313 **Figure 8.** Cyclic voltammograms for CA_1:2/GCE recorded at different scan rates (a,b) and

314 dependence of the peak current on the square roots of scan rate (c,d) in: 0.1 M NaOH (a,c) and

315 0.1 M PBS (b,d).

316 To determine the role of OH^- species in the formation of Ag_2O and its subsequent oxidation to

317 AgO, electrochemical experiments were conducted in an electrolyte with neutral pH – 0.1 M

318 PBS. The electrochemical behavior of the electrodes in this medium is also of particular interest

319 in terms of electrochemical sensors applied for the detection in blood (pH = 7.4). As can be seen

320 in Fig. 8b and Fig. S7b, only two small peaks were present. The anodic peak can be attributed to

321 the formation of silver (I) oxide because of the reaction between Ag^+ from silver sulfide and

322 hydroxyl groups adsorbed during the storage of the modified GCEs in the refrigerator suspended

323 over deionized water. Further positive scanning did not yield any peaks. The peak observed on

324 the cathodic curve may be correlated with the recovery of Ag_2S. The current values for both

peaks were proportional to the square root of the scan rate (Fig. 8d and Fig. S7d), indicating a diffusion-controlled process as also observed in 0.1 M NaOH. To further prove the origin of these peaks, repetitive cycling at 100 mV/s was carried out in both electrolytes. In the case of scanning in the alkaline medium, the current of peaks increased slightly (Fig. 9a). However, their potentials remained constant. Abd El Rehim et al. [10] assigned it to changes in surface roughness due to the reduction of the oxide layer. On the other hand, when the experiment was conducted in 0.1 M PBS, the peak currents decreased evidently suggesting consumption of available OH^- groups (Fig. 9b). The presented results indicate a perspective in boosting the electrocatalytic performance of CuS-based electrodes working at alkaline conditions with Ag_2S. In the case of electrochemical sensors, the formation of additional hydrous oxide species, which mediate the electrooxidation of biomolecules such as glucose [40] may improve the sensitivity of the electrodes.

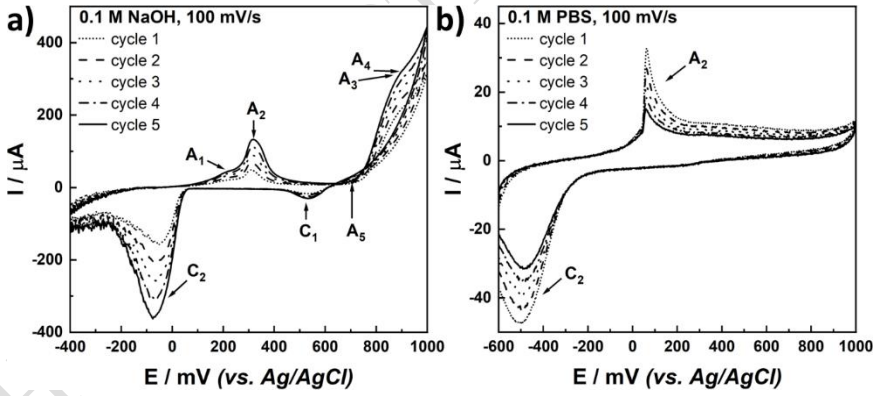

Figure 9. Cyclic voltammograms for CA_1:2/GCE recorded during repetitive cycling at 100 mV/s in: 0.1 M NaOH (a) and 0.1 M PBS (b).

4. Conclusions

In summary, a controlled and rapid chemical conversion route of CuS to Ag_2S at room temperature was proposed. It enabled to maintain the complex shape of the tube-like copper sulfide indicating its usefulness for the formation of silver sulfide particles with unusual

morphology. What is also important, our approach involved direct translation of the CuS to $AgNO_3$ ratio in the reaction solution into the final CuS:Ag_2S ratio in the product. Cyclic voltammetry measurements revealed that in contrast to CuS, the presence of silver sulfide yielded five anodic peaks and three cathodic peaks in an alkaline medium. They were ascribed to the formation of Ag-O bonds, Ag_2O and its subsequent oxidation. During the negative sweep, the reduction of AgO occurred, as well as the recovery of Ag_2S. The role of hydroxyl species in the formation of oxides was underlined by conducting experiments in 0.1 M PBS. Furthermore, it was proved that the converted Ag_2S exhibited similar electrochemical properties as a directly obtained one. The presented studies are of key importance for the interpretation of the electrochemical performance of the CuS and Ag_2S-based sensors planned in our future work. Additionally, the area of interest of the presented work can be further extended to photocatalysis and water splitting by proposing a facile route for the fabrication of CuS/Ag_2S heterostructures with controllable composition and complex morphology.

Funding: This research was funded in part by National Science Center, Poland, grant no. 2021/41/N/ST8/03515. Research project partially supported by program "Excellence initiative - research university" for the University of Science and Technology (J. M. M.).

References

[1] H. Li, X. Han, W. Zhao, A. Azhar, S. Jeong, D. Jeong, J. Na, S. Wang, J. Yu, Y. Yamauchi, Electrochemical preparation of nano/micron structure transition metal-based catalysts for the oxygen evolution reaction, Mater. Horizons. 9 (2022) 1788–1824. https://doi.org/10.1039/D2MH00075J.

[2] A. Das, B. Raj, M. Mohapatra, S.M. Andersen, S. Basu, Performance and future directions of transition metal sulfide-based electrode materials towards supercapacitor/supercapattery, Wiley Interdiscip. Rev. Energy Environ. 11 (2022) e414. https://doi.org/10.1002/wene.414.

[3] Y. Tang, T. Chen, S. Yu, Morphology controlled synthesis of monodispersed manganese sulfide nanocrystals and their primary application in supercapacitors with high performances, Chem. Commun. 51 (2015) 9018–9021. https://doi.org/10.1039/C5CC01700A.

[4] B. Dong, X. Zhao, G.Q. Han, X. Li, X. Shang, Y.R. Liu, W.H. Hu, Y.M. Chai, H. Zhao, C.G. Liu, Two-step synthesis of binary Ni-Fe sulfides supported on nickel foam as highly efficient electrocatalysts for the oxygen evolution reaction, J. Mater. Chem. A. 4 (2016) 13499–13508. https://doi.org/10.1039/c6ta03177c.

[5] S. Cheng, R. Zhang, W. Zhu, W. Ke, E. Li, CoS nanowires mediated by superionic conductor Ag_2S for boosted oxygen evolution, Appl. Surf. Sci. 518 (2020) 146106. https://doi.org/10.1016/j.apsusc.2020.146106.

[6] X. Rui, H. Tan, Q. Yan, Nanostructured metal sulfides for energy storage, Nanoscale. 6 (2014) 9889–9924. https://doi.org/10.1039/c4nr03057e.

[7] K.E. Toghill, R.G. Compton, Electrochemical non-enzymatic glucose sensors: A

perspective and an evaluation, Int. J. Electrochem. Sci. 5 (2010) 1246–1301.

[8] L. Qiana, J. Maoa, X. Tiana, H. Yuanb, D. Xiaoa, In situ synthesis of CuS nanotubes on Cu electrode for sensitive nonenzymatic glucose sensor, Sensors Actuators, B Chem. 176 (2013) 952–959. https://doi.org/10.1016/j.snb.2012.09.076.

[9] D.W. Hwang, S. Lee, M. Seo, T.D. Chung, Recent advances in electrochemical non-enzymatic glucose sensors – A review, Anal. Chim. Acta. 1033 (2018) 1–34. https://doi.org/10.1016/j.aca.2018.05.051.

[10] S.S. Abd El Rehim, H.H. Hassan, M.A.M. Ibrahim, M.A. Amin, Electrochemical Behaviour of a Silver Electrode in NaOH Solutions, Monatshefte Für Chemie / Chem. Mon. 129 (1998) 1103–1117. https://doi.org/10.1007/PL00010123.

[11] B.M. Jović, V.D. Jović, G.R. Stafford, Electrochemical formation and characterization of silver (I) oxide, Mater. Sci. Forum. 352 (2000) 57–64. https://doi.org/10.4028/www.scientific.net/msf.352.57.

[12] N. Butwong, T. Kunawong, J.H.T. Luong, Simultaneous analysis of hydroquinone, arbutin, and ascorbyl glucoside using a nanocomposite of Ag@AgCl nanoparticles, Ag_2S nanoparticles, multiwall carbon nanotubes, and chitosan, Nanomaterials. 10 (2020) 1583. https://doi.org/10.3390/nano10081583.

[13] Y.C. Chen, Y.M. Bai, Y.K. Hsu, Biomarker detection for disease diagnosis via versatile Ag_2S nanowires as electrochemical sensor and SERS substrate, J. Alloys Compd. 881 (2021) 160647. https://doi.org/10.1016/j.jallcom.2021.160647.

[14] D. Wang, C. Hao, W. Zheng, Q. Peng, T. Wang, Z. Liao, D. Yu, Y. Li, Ultralong single-crystalline Ag_2S nanowires: Promising candidates for photoswitches and room-temperature oxygen sensors, Adv. Mater. 20 (2008) 2628–2632.

https://doi.org/10.1002/adma.200800138.

[15] A.-R. Jang, J.E. Lim, S. Jang, M.H. Kang, G. Lee, H. Chang, E. Kim, J.K. Park, J.-O. Lee, Ag_2S nanoparticles decorated graphene as a selective chemical sensor for acetone working at room temperature, Appl. Surf. Sci. 562 (2021) 150201. https://doi.org/10.1016/j.apsusc.2021.150201.

[16] W. Yu, J. Yin, Y. Li, B. Lai, T. Jiang, Y. Li, H. Liu, J. Liu, C. Zhao, S.C. Singh, J. Chen, B. Lin, H. Idriss, C. Guo, Ag_2S Quantum Dots as an Infrared Excited Photocatalyst for Hydrogen Production, ACS Appl. Energy Mater. 2 (2019) 2751–2759. https://doi.org/10.1021/acsaem.9b00091.

[17] S. Wageh, A.A. Al-Ghamdi, A. Numan, J. Iqbal, Silver sulfide nanoparticles incorporated into graphene oxide: an efficient electrocatalyst for the oxygen reduction reaction, J. Mater. Sci. Mater. Electron. 31 (2020) 8127–8135. https://doi.org/10.1007/s10854-020-03409-4.

[18] H. Ren, W. Xu, S. Zhu, Z. Cui, X. Yang, A. Inoue, Synthesis and properties of nanoporous Ag_2S/CuS catalyst for hydrogen evolution reaction, Electrochim. Acta. 190 (2016) 221–228. https://doi.org/10.1016/j.electacta.2015.12.096.

[19] X. Xia, X. Zhao, W. Ye, C. Wang, Highly porous Ag-Ag_2S/MoS_2 with additional active sites synthesized by chemical etching method for enhanced electrocatalytic hydrogen evolution, Electrochim. Acta. 142 (2014) 173–181. https://doi.org/10.1016/j.electacta.2014.07.129.

[20] M. Wang, P. Ju, W. Li, Y. Zhao, X. Han, Ag_2S nanoparticle-decorated MoS_2 for enhanced electrocatalytic and photoelectrocatalytic activity in water splitting, Dalt. Trans. 46 (2017) 483–490. https://doi.org/10.1039/c6dt04079a.

[21] A. Kusior, A. Trenczek-Zajac, J. Mazurków, K. Michalec, M. Synowiec, M. Radecka, Chapter Ten - Interface design, surface-related properties, and their role in interfacial electron transfer. Part I: Materials-related topics, in: R. van Eldik, C.D. Hubbard (Eds.), Adv. Inorg. Chem., Elsevier, 2022: pp. 373–409. https://doi.org/10.1016/bs.adioch.2021.12.005.

[22] A. Trenczek-Zajac, A. Kusior, J. Mazurków, K. Michalec, M. Synowiec, M. Radecka, Chapter Eleven - Interface design, surface-related properties, and their role in interfacial electron transfer. Part II: Photochemistry-related topics, in: R. van Eldik, C.D. Hubbard (Eds.), Adv. Inorg. Chem., Elsevier, 2022: pp. 411–442. https://doi.org/10.1016/bs.adioch.2021.12.010.

[23] M. Basu, R. Nazir, C. Mahala, P. Fageria, S. Chaudhary, S. Gangopadhyay, S. Pande, Ag_2S/Ag Heterostructure: A Promising Electrocatalyst for the Hydrogen Evolution Reaction, Langmuir. 33 (2017) 3178–3186. https://doi.org/10.1021/acs.langmuir.7b00029.

[24] C. Tan, C. Hsiao, S. Wang, P. Liu, M. Lu, M.H. Huang, H. Ouyang, L. Chen, Sequential Cation Exchange Generated Superlattice Nanowires Forming Multiple p-n Heterojunctions, ACSNano. 8 (2014) 9422–9426.

[25] J. Kundu, D. Pradhan, Controlled synthesis and catalytic activity of copper sulfide nanostructured assemblies with different morphologies, ACS Appl. Mater. Interfaces. 6 (2014) 1823–1834. https://doi.org/10.1021/am404829g.

[26] J.M. Mazurków, A. Kusior, M. Radecka, Electrochemical characterization of modified glassy carbon electrodes for non-enzymatic glucose sensors, Sensors. 21 (2021) 7928. https://doi.org/10.3390/s21237928.

[27] I. Martina, R. Wiesinger, D. Jembrih-Simbuerger, M. Schreiner, Micro-Raman

Characterisation of Silver Corrosion Products: Instrumental Set Up and Reference Database, E-Preservation Sci. 9 (2012) 1–8.

[28] J.F. Moulder, W.F. Stickle, P.E. Sobol, K.D. Bomben, Handbook of X-ray Photoelectron Spectroscopy, Physical Electronics Division, Perkin-Elmer Corporation, Eden Prairie, Minnesota, USA, 1992.

[29] A.M. Ferraria, A.P. Carapeto, A.M. Botelho Do Rego, X-ray photoelectron spectroscopy: Silver salts revisited, Vacuum. 86 (2012) 1988–1991. https://doi.org/10.1016/j.vacuum.2012.05.031.

[30] Y. Xie, A. Riedinger, M. Prato, A. Casu, A. Genovese, P. Guardia, S. Sottini, C. Sangregorio, K. Miszta, S. Ghosh, T. Pellegrino, L. Manna, Copper sulfide nanocrystals with tunable composition by reduction of covellite nanocrystals with Cu^{+} ions, J. Am. Chem. Soc. 135 (2013) 17630–17637. https://doi.org/10.1021/ja409754v.

[31] M. Fantauzzi, B. Elsener, D. Atzei, A. Rigoldi, A. Rossi, Exploiting XPS for the identification of sulfides and polysulfides, RSC Adv. 5 (2015) 75953–75963. https://doi.org/10.1039/c5ra14915k.

[32] C. Du, Y. Zhu, Z. Wang, L. Wang, W. Younas, X. Ma, C. Cao, Cuprous Self-Doping Regulated Mesoporous CuS Nanotube Cathode Materials for Rechargeable Magnesium Batteries, ACS Appl. Mater. Interfaces. 12 (2020) 35035–35042. https://doi.org/10.1021/acsami.0c09466.

[33] C. Luo, Y. Zhang, X. Zeng, Y. Zeng, Y. Wang, The role of poly(ethylene glycol) in the formation of silver nanoparticles, J. Colloid Interface Sci. 288 (2005) 444–448. https://doi.org/10.1016/j.jcis.2005.03.005.

[34] Y. Shi, Y. Chen, G. Tian, L. Wang, Y. Xiao, H. Fu, Hierarchical Ag/Ag_2S/CuS Ternary

Heterostructure Composite as an Efficient Visible-Light Photocatalyst, ChemCatChem. 7 (2015) 1684–1690. https://doi.org/10.1002/cctc.201500121.

[35] L. Motte, J. Urban, Silver Clusters on Silver Sulfide Nanocrystals: Synthesis and Behavior after Electron Beam Irradiation, J. Phys. Chem. B. 109 (2005) 21499–21501. https://doi.org/10.1021/jp0542322.

[36] F.H. Assaf, A.M. Zaky, S.S. Abd El-Rehim, Cyclic voltammetric studies of the electrochemical behaviour of copper-silver alloys in NaOH solution, Appl. Surf. Sci. 187 (2002) 18–27. https://doi.org/10.1016/S0169-4332(01)00462-7.

[37] H. Luo, X. Ji, S. Cheng, Investigation into the electrochemical behaviour of silver in alkaline solution and the influence of Au-decoration using: Operando Raman spectroscopy, RSC Adv. 10 (2020) 8453–8459. https://doi.org/10.1039/c9ra10282e.

[38] A.M. Zaky, S.S.A. El Rehim, B.M. Mohamed, Electrochemical behaviour of polycrystalline silver in 0.5M NaOH containing sulphide ions, Corros. Eng. Sci. Technol. 40 (2005) 21–27. https://doi.org/10.1179/174327805X29903.

[39] D.M.E. Garcia, A.S.T.M. Pereira, A.C. Almeida, U.S. Roma, A.B.A. Soler, P.D. Lacharmoise, I.M. Das Mercês Ferreira, C.C.D. Simaõ, Large-Area Paper Batteries with Ag and Zn/Ag Screen-Printed Electrodes, ACS Omega. 4 (2019) 16781–16788. https://doi.org/10.1021/acsomega.9b01545.

[40] L.D. Burke, Premonolayer oxidation and its role in electrocatalysis, Electrochim. Acta. 39 (1994) 1841–1848. https://doi.org/10.1016/0013-4686(94)85173-5.